Quantum Crosstalk Robust Quantum Control

Zeyuan Zhou,[1] Ryan Sitler,[2] Yasuo Oda[ORCID],[1] Kevin Schultz[ORCID],[2] and Gregory Quiroz[ORCID][1,2,*]

[1]*William H. Miller III Department of Physics & Astronomy, Johns Hopkins University, Baltimore, Maryland 21218, USA*
[2]*Johns Hopkins University Applied Physics Laboratory, Laurel, Maryland 20723, USA*

The prevalence of quantum crosstalk in current quantum devices poses challenges for achieving high-fidelity quantum logic operations and reliable quantum processing. Through quantum control theory, we develop an analytical condition for achieving crosstalk-robust single-qubit control of multiqubit systems. We examine the effects of quantum crosstalk via a cumulant expansion and develop a condition to suppress the leading order contributions to the dynamics. The efficacy of the condition is illustrated in the domains of quantum state preservation and noise characterization through the development of crosstalk-robust dynamical decoupling and quantum noise spectroscopy (QNS) protocols. Using the IBM Quantum Experience, crosstalk-robust state preservation is demonstrated on 27 qubits, where up to a $3.5\times$ improvement in coherence decay is observed for single-qubit product and multipartite entangled states. Through the use of noise injection, we demonstrate crosstalk-robust dephasing QNS on a seven qubit processor, where a 10^4 improvement in reconstruction accuracy over alternative protocols is found. Together, these experiments highlight the significant impact the crosstalk suppression condition can have on improving multiqubit characterization and control on current quantum devices.

Introduction.—The ability to implement high-fidelity quantum logic operations is a necessity for achieving reliable and scalable quantum computing [1]. In current systems, however, system-environment interactions and crosstalk are typically quite substantial and ultimately limit qubit coherence and gate fidelities. Characterized as unwanted interqubit coupling, quantum crosstalk causes undesired dynamics that violate the locality and individual addressability of qubits. It is known to be prevalent in current systems and presents obstacles in the implementation of quantum algorithms [2–6], quantum characterization [7–10], and instantiations of quantum error correction [11,12].

Quantum crosstalk arises in a variety of qubit architectures. Atomic systems are susceptible to unwanted interactions between neighboring spectator qubits during two-qubit operations [12–17], while superconductor (e.g., fixed-frequency transmons [18–21]) and semiconductor [22–24] platforms commonly experience parasitic ZZ interactions from always-on coupling used to implement entangling gates. Various strategies have been proposed to address crosstalk from the hardware and software perspective. Hardware solutions have predominately centered around architecture design [25–27]. Software approaches are diverse and have sought to address crosstalk at the physical [6,17,22,28–30] and compiler [2,3,31,32] layers of the quantum software stack. Despite their utility, these approaches are either hardware specific or provide limited insight and intuition into broader principles for crosstalk suppression.

We address this challenge by leveraging quantum control theory to develop an analytical condition for achieving crosstalk-robust (CR) single-qubit control of multiqubit systems. Quantum control is widely used for constructing high-fidelity gates [33–38] and error suppression strategies [39–42], as well as unraveling key characteristics of spatiotemporally correlated noise through quantum noise spectroscopy (QNS) [43–51]. We exploit a control framework commonly used to derive the filter function formalism [34,35,47,52–54] to examine the impact of crosstalk on system dynamics. Through the use of a perturbative cumulant-based expansion, we derive a control condition that enables quantum crosstalk cancellation up to first order in the total evolution time.

The versatility and applicability of our approach is illustrated through experimental investigations of CR quantum state preservation and noise characterization on the IBM Quantum Experience (IBMQE). CR dynamical decoupling (CRDD) is introduced and shown to dramatically improve the simultaneous preservation of single-qubit product states (SPSs) and multipartite entangled states (MESs) up to 27 qubits. Furthermore, we demonstrate the relevance of the condition to noise characterization,

where a CR dephasing QNS protocol is introduced and subsequently used to perform the first known simultaneous noise spectrum estimation on seven qubits. Together, these experiments highlight the deleterious effects of crosstalk and the remarkable impact our condition can have on improving multiqubit characterization and control on current quantum devices.

Crosstalk noise model.—We focus on the suppression of crosstalk during the implementation of single qubit operations as this represents the most fundamental type of control one may possess on a quantum system. To this end, we consider an N-qubit system subject to noisy, controlled evolution governed by the time-dependent Hamiltonian $H(t) = H_C(t) + H_E(t)$. The control Hamiltonian is given by

$$H_C(t) = \sum_{i=1}^{N} \frac{\Omega_i(t)}{2} [\sigma_i^x \cos \phi_i(t) + \sigma_i^y \sin \phi_i(t)], \quad (1)$$

where $\Omega_i(t)$ and $\phi_i(t)$ represent the time-dependent control amplitude and phase, respectively. Noise is generated by the error Hamiltonian

$$H_E(t) = \sum_{i=1}^{N} \vec{\sigma}_i \cdot \vec{\beta}_i(t) + \sum_{i<j}^{N} J_{ij} \sigma_i^z \sigma_j^z. \quad (2)$$

The first term describes semiclassical, spatiotemporally correlated noise with $\vec{\sigma}_i = (\sigma_i^x, \sigma_i^y, \sigma_i^z)$ consisting of the ith qubit Pauli operators and $\vec{\beta}_i(t) = (\beta_i^x(t), \beta_i^y(t), \beta_i^z(t))$. $\beta_i^\mu(t)$ is assumed to be a wide-sense stationary Gaussian stochastic process with zero-mean, $\overline{\beta_i^\mu(t)} = 0$, and two-point correlation functions $C_{ij}^{\mu\nu}(\tau) = \overline{\beta_i^\mu(\tau)\beta_j^\nu(0)}, \mu, \nu = x, y, z$. Note that $\overline{\cdots}$ denotes classical ensemble averaging. The model also includes quantum crosstalk that is characterized by the static coupling strength J_{ij} and two local ZZ interactions on the ith and jth qubits. This model and its generalization described in the Supplemental Material [55] are relevant to a wide range of experimental platforms, including superconducting qubits [18,19,26,44], semiconductor qubits [22,23,61,62], and trapped ion systems [12,13,17,48,50,63].

Effective error dynamics.—We investigate the effect of $H_E(t)$ on the dynamics of expectation values and state fidelity. The evolution generated by the error Hamiltonian is isolated by moving into the interaction (toggling) frame with respect to the control such that the total evolution is described by $U(T) = \tilde{U}_E(T,0)U_C(T,0)$. The propagator $U_C(T,0) = \mathcal{T}_+ e^{-i\int_0^T dt H_C(t)}$ describes the control dynamics, while $\tilde{U}_E(T,0) = \mathcal{T}_+ e^{-i\int_0^T dt \tilde{H}_E(t)}$ is the rotated-frame time evolution governed by $\tilde{H}_E(t) = U_C(T,t)H_E(t)U_C^\dagger(T,t); \mathcal{T}_+$ denotes the time-ordering operator. The rotated-frame error Hamiltonian is further specified by

$$\tilde{H}_E(t) = \sum_{i=1}^{N} \vec{\Lambda}_i(t) \cdot \vec{\beta}_i(t) + \sum_{i<j}^{N} J_{ij}[\vec{\Lambda}_i^T(t)]_z [\vec{\Lambda}_j(t)]_z, \quad (3)$$

where $\vec{\Lambda}_i(t) \equiv \mathbf{R}_i(t)\vec{\sigma}_i^T$ and $\mathbf{R}_i(t)$ is the "control matrix" with elements $R_i^{\mu\nu}(t) = \text{Tr}[U_C(T,t)\sigma_i^\mu U_C^\dagger(T,t)\sigma_i^\nu]/2$. A^T and $[\vec{a}]_z$ denote the transpose of A and the z component of $\vec{a}$, respectively.

We quantify the impact of noise on the time-dependent expectation value of an observable O using a cumulant-based perturbative expansion [47,64]. In the strong control and weak noise limit [47,54,64], where $H_C(t)$ dominates the dynamics and $H_E(t)$ is treated as a perturbation, the noise-averaged expectation value $\overline{\langle O(T) \rangle} = \overline{\text{Tr}[\rho(T)O]}$ with respect to the time-evolved state $\rho(T) = U(T)\rho(0)U^\dagger(T)$ can be approximated as

$$\overline{\langle O(T) \rangle} \approx \text{Tr}[e^{-i\mathcal{C}_O^{(1)}(T) - \mathcal{C}_O^{(2)}(T)/2}\rho_C(T)O]. \quad (4)$$

$\rho_C(T,0) = U_C(T,0)\rho(0)U_C^\dagger(T,0)$ represents the time-evolved state with respect to the ideal control dynamics, while the error dynamics generated by $H_E(t)$ are described by the first and second cumulants:

$$\mathcal{C}_O^{(1)}(T) = \sum_{i<j}^{N} \sum_{\mu,\nu=x,y,z} \chi_{ij}^{\mu\nu}(T)(\sigma_i^\mu \sigma_j^\nu - O^{-1}\sigma_i^\mu \sigma_j^\nu O), \quad (5)$$

$$\mathcal{C}_O^{(2)}(T) = \sum_{i,j=1}^{N} \sum_{\nu,\gamma=x,y,z} \Gamma_{ij}^{\nu\gamma}(T)\mathcal{A}_{ij}^{\nu\gamma}, \quad (6)$$

where $\mathcal{A}_{ij}^{\nu\gamma} = \sigma_i^\nu \sigma_j^\gamma + O^{-1}\sigma_i^\nu \sigma_j^\gamma O - O^{-1}\sigma_i^\nu O\sigma_j^\gamma - \sigma_i^\nu O^{-1}\sigma_j^\gamma O$. $\mathcal{C}_O^{(1)}(T)$ and $\mathcal{C}_O^{(2)}(T)$ are proportional to the mean and variance of the noise, respectively. Consequently, the cumulants are determined by the overlap integrals

$$\chi_{ij}^{\mu\nu}(T) \equiv J_{ij} \int_0^T R_i^{z\mu}(t)R_j^{z\nu}(t)dt, \quad (7)$$

$$\Gamma_{ij}^{\nu\gamma}(T) \equiv \sum_{\mu,\delta=x,y,z} \int_0^\infty \frac{d\omega}{2\pi} \mathcal{G}_{ij}^{\mu\nu\delta\gamma}(\omega,T)S_{ij}^{\mu\delta}(\omega), \quad (8)$$

where $\chi_{ij}^{\mu\nu}(T)$ is due to crosstalk and $\Gamma_{ij}^{\nu\gamma}(T)$ captures the temporally correlated noise. $S_{ij}^{\mu\nu}(\omega) = \int_0^T C_{ij}^{\mu\nu}(\tau)e^{-i\omega\tau}dt$ designates the noise power spectral density. The filter functions $\mathcal{G}_{ij}^{\mu\nu\delta\gamma}(\omega,T) \equiv \text{Re}[G_i^{\mu\nu}(\omega,T)G_j^{\delta\gamma}(-\omega,T)]$ are defined in terms of the Fourier transforms of the elements of the control matrix: $G_i^{\mu\nu}(\omega,T) \equiv \int_0^T R_i^{\mu\nu}(t)e^{i\omega t}dt$.

Similar expressions can be obtained for the fidelity (i.e., overlap) between the initial state $\rho(0)$ and time-evolved state $\rho(T)$. When $\rho(0)$ is a pure state, the noise-averaged fidelity is given by $\mathcal{F}(T) = \overline{\text{Tr}[\rho(T)\rho(0)]}$. In general, $\rho(0)$

can be noninvertible which poses challenges for recasting $\mathcal{F}(T)$ in the form of Eq. (4) [55]. However, by expanding the initial state as a sum of invertible, Hermitian operators, $\rho(0) = \sum_\ell \Phi_\ell$, the fidelity becomes

$$\mathcal{F}(T) \approx \sum_\ell \mathrm{Tr}[e^{-i\mathcal{C}_{\Phi_\ell}^{(1)}(T) - \mathcal{C}_{\Phi_\ell}^{(2)}(T)/2} \rho_C(T) \Phi_\ell]. \qquad (9)$$

In the case of qubit systems, Φ_i may be chosen to be proportional to the N-qubit Pauli operators. Note that the cumulant expressions of Eq. (9) only differ from Eq. (4) by operator conjugations.

Crosstalk-robust control condition.—In the cumulant representation, a control protocol defined by $\{\Omega_i(t), \phi_i(t)\}_{i=1}^N$ attains nth order suppression of the error dynamics when $\mathcal{C}_O^{(k)}(T) = 0$ for $k \leq n$. Suppression of the first cumulant is achieved by cancellation of the pure crosstalk contribution, or more specifically, satisfying the *crosstalk suppression condition* (CSC):

$$\chi_{ij}^{\mu\nu}(T) = 0 \quad \forall \ i, j, \mu, \nu; \qquad (10)$$

a multiaxis generalization is included in the Supplemental Material [55]. Second-order suppression is imposed via Eq. (10) in conjunction with minimizing the spectral overlap between the system-environment noise and the filter functions $\forall \ i, j, \nu, \gamma$.

The efficacy of the above condition is explored in the next sections via demonstrations of quantum state preservation and QNS on the IBMQE. Composed of fixed-frequency transmons, IBMQE processors are susceptible to parasitic ZZ crosstalk [7,19,30] and temporally correlated noise [30,65–68], both of which are captured by Eq. (2). Thus, they present suitable testbeds for evaluating and showcasing the potential benefit of imposing Eq. (10).

Quantum state preservation.—We demonstrate the utility of the CSC in the context of quantum state preservation through the design and evaluation of CRDD. DD selectively averages out unwanted interactions between a quantum system and its environment through the use of fast and strong pulses [41]. When properly designed, DD preserves the state of a single qubit system, while suppressing static quantum crosstalk [30]. Here, we show how the CSC enables greater generality for simultaneous preservation of an array of qubits initialized in SPSs and MESs.

While the CSC permits a diverse family of possible CRDD protocols, for concreteness, we focus on those inspired by XY4 [39]. This sequence utilizes repetitions of $f_\tau X f_\tau Y f_\tau X f_\tau Y$, where X and Y are π pulses (of duration δ) about the x and y axis of the single qubit Bloch sphere, respectively. Free evolution periods f_τ, where the system evolves according to its internal dynamics, are of duration τ; thus, yielding a cycle time of $t_{XY4} = 4(\tau + \delta)$. XY4 affords
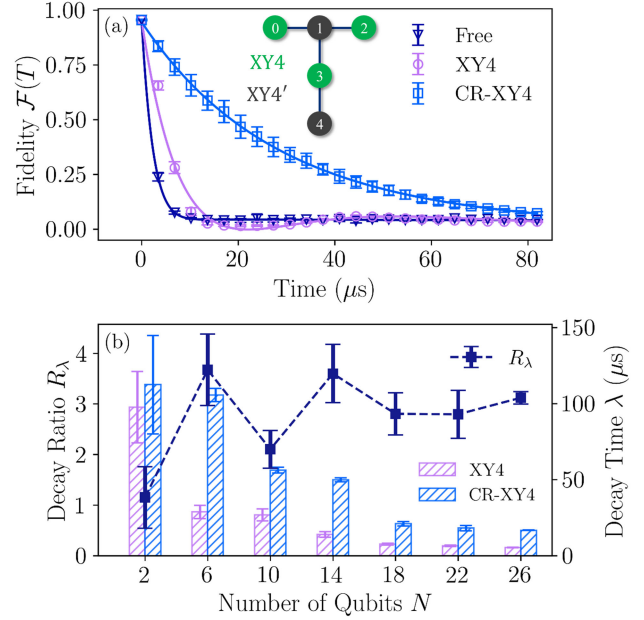

FIG. 1. Simultaneous preservation of SPSs using different control protocols. (a) Fidelity vs time for the IBMQE Lima 5-qubit processor using free evolution (dark blue down-triangles), XY4 (light purple circles), and CR-XY4 (light blue squares). Data points and error bars denote mean fidelity and CIs, respectively, obtained from bootstrapping. Inset: CR-XY4 protocol on IBMQE Lima; similar patterning used for IBMQE Auckland. (b) Fidelity decay rate comparison between XY4 and CR-XY4 using up to 26 qubits on IBMQE Auckland. Bars represent mean decay time λ (with CI error bars), while the line signifies R_λ. Results are collected using the same procedure outlined for the top panel. In both cases, CR-XY4 exhibits significant improvement over XY4.

suppression of system-environment interactions to first order in time-dependent perturbation theory [39].

CR state preservation is achieved by properly adjusting the pulse locations of multiqubit variants of XY4. Given an array of qubits, the CSC is enforced by patterning two sequences across the array: XY4 and $XY4' = Xf_\tau Yf_\tau Xf_\tau Yf_\tau$; this protocol is labeled CR-XY4. An example of the protocol is shown in the inset of Fig. 1(a). Achieving universal single-qubit decoupling in the ideal pulse limit, CR-XY4 affords crosstalk suppression when $\tau = \delta$ (i.e., pulse-width effects are significant). In the DD context, the suppression condition is equivalent to enforcing the typical anticommutativity required to achieve first-order decoupling [41]. As such, variants of CRDD based on time-symmetric XY4 [69] and Eulerian DD [70] may be considered as well.

CR-XY4 is evaluated against free evolution and XY4. The three protocols are compared by simultaneously preparing N qubits in the state $|\Psi\rangle = \otimes_{i=1}^N |\psi_i\rangle$, where $|\psi_i\rangle$ is the ith-qubit state. We focus on states in the xy plane as these are among the most susceptible to ZZ crosstalk. State preparation is followed by M repetitions of XY4 or CR-XY4 (or the free evolution equivalent), applied for a

total time $T = M t_{\text{XY4}} = M t_{\text{CR-XY4}}$. For all devices discussed below, $\tau = \delta = 35$ ns. The circuit is completed by applying the inverse state preparation unitary followed by a measurement in the computational basis. Resulting measurements are used to estimate the fidelity $\mathcal{F}(T)$ between $\rho(0) = |\Psi\rangle\langle\Psi|$ and $\rho(T)$ resulting from free or DD evolution.

CR-XY4 substantially improves the fidelity of SPSs. In Fig. 1(a), a comparison between the protocols is shown for the IBMQE Lima 5-qubit processor. Estimates of average fidelity and 95% confidence intervals (CIs) are determined via bootstrapping [71] from 1000 resamples of data collected from 20 random qubit states in the xy plane, 8000 shots, and four replicates of the experiment run over four days. The data is fit to the modified exponential decay [42]: $F(t) = c[1 - f(t)] + F_0$, where $f(t) = 1/(1 + k)[k e^{-t/\lambda} \times \cos(t\gamma) + e^{-t/\alpha}]$, and $c = (F_{T_{\max}} - F_0)/[f(T_{\max}) - 1]$. The model includes short and long decay times λ and α, respectively, oscillation frequency γ, and dimensionless weight parameter k. The fidelity at $M = 0$ and $M = M_{\max}$ are given by F_0 and $F_{T_{\max}}$.

A comparison of the short decay times via the ratio $R_\lambda = \lambda_{\text{CR-XY4}}/\lambda_{\text{XY4}}$ reveals a near factor of 4 improvement for CR-XY4 over XY4. The abrupt change in R_λ at $N = 6$ is due to a rapid accumulation in crosstalk for XY4; see the Supplemental Material [55] for further details. We attribute hardware variability, and the presence of nonlocal crosstalk to the fluctuations in $\lambda_{\text{CR-XY4}}$ thereafter.

CR-XY4 considerably enhances the time-average fidelity of MESs. In Fig. 2, N qubits are simultaneously prepared in K' entangled states and then subject to M repetitions of XY4 or CR-XY4. Then, prior to measurement in the computational basis, the inverse state preparation unitary is applied. Upon applying up to $M_{\max} = 50$ repetitions of DD, the time-averaged fidelity $\mathcal{F}_{\text{avg}} = T_{\max}^{-1} \int_0^{T_{\max}} [\mathcal{F}(t)/\mathcal{F}(0)] dt$ is calculated via numerical integration for each DD protocol [72]. Note that $\mathcal{F}_{\text{avg}}$ captures long-time behavior, with the normalization accounting for state preparation errors. $\mathcal{F}_{\text{avg}}$ is conditioned on the simultaneous preservation of $K \leq K'$ states on physically adjacent qubits. We consider $N = 20$ qubits simultaneously prepared in $K' = 10$ Bell states of the form $|\Phi_\pm\rangle = 1/\sqrt{2}(|00\rangle \pm |11\rangle)$ or $|\Psi_\pm\rangle = 1/\sqrt{2}(|01\rangle \pm |10\rangle)$. A similar procedure is used for the three-qubit W state $|W\rangle = 1/\sqrt{3}(|001\rangle + |010\rangle + |100\rangle)$, where $K' = 9$ entangled states are prepared on $N = 27$ qubits. In Fig. 2, the fidelity ratio $R_{\mathcal{F}} = \mathcal{F}_{\text{avg}}^{\text{CR-XY4}}/\mathcal{F}_{\text{avg}}^{\text{XY4}}$ is shown for both state preparations. $\mathcal{F}_{\text{avg}}$ collected from all qubit configurations for a given K and initial states, 8000 shots, and five replicates of the experiments are used to estimate $R_{\mathcal{F}}$ averages and CIs via bootstrapping.

Individual Bell states are invariant under ZZ crosstalk; however, multiple Bell states prepared physically adjacent on the quantum device experience ZZ crosstalk across the
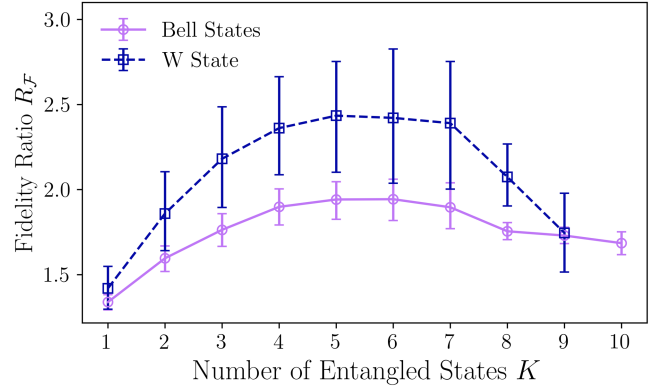

FIG. 2. Ratio of time-averaged fidelities of CR-XY4 and XY4 for the simultaneous protection of K MESs on the 27-qubit IBMQE Auckland processor. Bell state (light purple circles) results are collected using 8000 shots, the four Bell states, and five replicates of the experiment collected over five days. Similar data is collected for the W state (dark blue squares). Averages and CIs are determined by bootstrapping, using 1000 resamples of the data. Results indicate CR-XY4 improves state preservation over XY4 for both cases.

common edge. The impact of suppressing edge effects is observed via the near $2\times$ improvement over XY4 obtained by CR-XY4. The W state does not possess inherent robustness and therefore experiences a greater benefit from CRDD: a $2.5\times$ improvement. Despite the increasing contributions from state preparation, measurement, and gate error observed at large N, CR-XY4 achieves a slower decay in fidelity than XY4; hence, a higher time-averaged fidelity for both MES preparations considered.

Quantum noise spectroscopy.—In QNS, a controlled quantum system is used as a dynamical probe to characterize the spectral properties of environmental noise. Under the zero-mean noise assumption, QNS typically involves constructing a linear inversion problem via Eq. (8) to determine $S_{ij}^{\mu\delta}(\omega)$ from carefully engineered filter functions and estimates of expectation value decay rates. This assumption is violated in the presence of static crosstalk, where unwanted contributions from $\mathcal{C}_O^{(1)}(T)$ result in deviations from the expected dynamics. As we show below, crosstalk suppression is key to enabling simultaneous single-qubit QNS on a collection of qubits.

Using the CSC, we design a CR variant of the fixed total time pulse sequences (FTTPS) [73,74], i.e., CR-FTTPS to perform dephasing QNS. Bookended by two $X_{\pi/2}$ pulses, FTTPS consist of $\ell/2$ distinct sequences, each containing ℓ gates. In the instantaneous pulse limit, the κth sequence of "cosine" FTTPS yields the discrete-time control matrix $R_{i,\kappa}^{zz}(m) = \text{sgn}\{\cos(\pi\kappa m/\ell)\}$ for $m = 1, \ldots, \ell$. Sign changes in the cosine function denote locations of X gates and I gates otherwise. Simultaneous application of "cosine" FTTPS (S-FTTPS) on multiple qubits does not cancel the first cumulant and therefore will be sensitive to
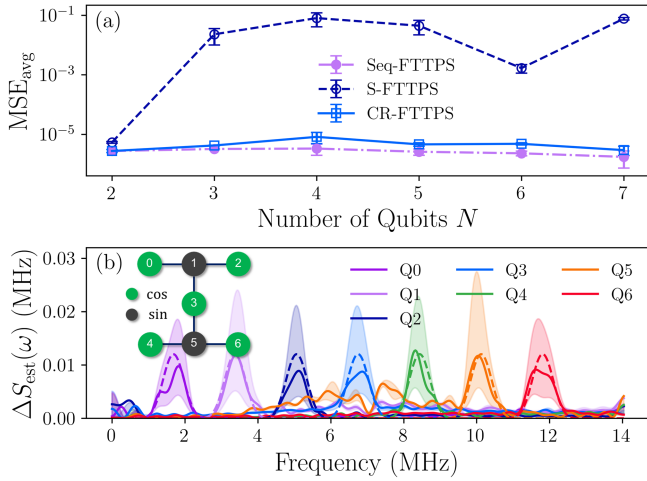
FIG. 3. CR-QNS on the 7-qubit IBMQE Nairobi processor, where narrow band dephasing noise with distinct center frequencies is injected on each qubit. (a) Reconstruction error as a function of the number of qubits for FTTPS variants. Data points denote averages and error bars are CIs. CR-FTTPS outperforms S-FTTPS by up to 4 orders of magnitude. (b) Seven-qubit simultaneous local dephasing QNS using CR-FTTPS. Average spectrum estimates (solid lines) and CIs (shaded regions) indicate good agreement with injected noise (dashed lines). Inset: CR-FTTPS protocol on Nairobi. Averages and CIs are determined from bootstrapping.

crosstalk. CR-FTTPS is attained via an additional "sine" FTTPS described by $R_{i,\kappa}^{zz}(m) = \text{sgn}\{\sin(\pi\kappa m/\ell)\}$ and alternating the qubit array with the cosine and sine variants of FTTPS.

Using the IBMQE Nairobi 7-qubit processor, we inject narrow band dephasing noise at N distinct frequencies on N qubits via the Schrödinger wave moving average model (SchWARMA) approach [74]. Three variants of FTTPS are considered: S-FTTPS, CR-FTTPS, and Seq-FTTPS, where FTTPS is applied sequentially to all qubits. In Fig. 3(a), we examine the qubit-averaged mean-squared error $\text{MSE}_{\text{avg}} = (2/N\ell)\sum_{i=1}^{N}\sum_{k=0}^{\ell/2-1}[\Delta S_{\text{est},i}(\omega_k) - S_i(\omega_k)]^2$ for each protocol over $\ell/2$ discrete frequencies $\omega_k = k\pi/T$. The total time is $T = \ell\tau$, where τ is the gate time. The residual spectrum $\Delta S_{\text{est},i}(\omega) = S_{\text{est},i}(\omega) - \hat{S}_{\text{est},i}(\omega)$ captures the injected noise $S_i(\omega)$ and crosstalk not present in the Seq-FTTPS native background spectrum $\hat{S}_{\text{est},i}(\omega)$. Five datasets are collected over five days for $\ell = 128$ using 10 SchWARMA trajectories and $\tau = 35$ ns gates. Bootstrapped spectrum estimates and CIs are determined from 1000 resamples of the reconstructed spectra.

While all protocols perform similarly for $N = 2$, we observe a sudden degradation in S-FTTPS performance thereafter. We attribute this effect to crosstalk, which leads to an effective ith-qubit decay rate of $\tilde{\Gamma}_{ii}^{zz} = \Gamma_{ii}^{zz} + \sum_{j=1}^{N}\ln|\cos(J_{ij}T)|$. The vertical shift in the decay rate ultimately manifests as a raised white noise floor in $S_{ii}^{zz}(\omega)$

that conceals characteristics of the injected and native spectra; thus, significantly reducing reconstruction accuracy.

In contrast, CR-FTTPS exhibits reconstruction accuracy nearly equivalent to Seq-FTTPS. The discrepancy between the two protocols arises from finite-width pulse effects during the X gates that result in small violations of the CSC. This effect manifests as spurious features in the reconstructions around 4–10 MHz. Figure 3(b) showcases a demonstration of CR-FTTPS on $N = 7$ qubits—the largest known simultaneous single-qubit dephasing QNS demonstration to date—where such features can be observed; this is the largest known simultaneous single-qubit dephasing QNS demonstration to date. Note that despite the deviations, average estimates (solid lines) and CIs (shaded regions) agree remarkably well with the injected spectra (dotted lines).

Conclusions.—Through the lens of quantum control, we develop a condition for first-order quantum crosstalk suppression for general single qubit control of multiqubit systems. The utility of the condition is demonstrated in the domains of quantum state preservation and noise characterization, where we design crosstalk-robust DD and QNS, respectively. Through demonstrations on the IBMQE, we showcase the significance of the condition in each domain on various processors, simultaneously suppressing crosstalk on up to 27 qubits. Together, these experiments highlight the crucial impact our condition can have on improving the scalability of characterization and control on current quantum devices.

[*]Corresponding author: Gregory.Quiroz@jhuapl.edu

[1] J. Preskill, Quantum **2,** 79 (2018).

[2] Y. Ding, P. Gokhale, S. F. Lin, R. Rines, T. Propson, and F. T. Chong, in *Proceedings of the 2020 53rd Annual IEEE/ ACM International Symposium on Microarchitecture (MICRO)* (IEEE, New York, 2020).

[3] P. Murali, D. C. Mckay, M. Martonosi, and A. Javadi-Abhari, in *Proceedings of the Twenty-Fifth International Conference on Architectural Support for Programming Languages and Operating Systems* (2020), 10.1145/3373376.3378477.

[4] D. V. Babukhin and W. V. Pogosov, Quantum Inf. Process. **21,** 7 (2022).

[5] Y. Ohkura, T. Satoh, and R. Van Meter, IEEE Trans. Quantum Eng. **3,** 1 (2022).

[6] L. Xie, J. Zhai, Z. Zhang, J. Allcock, S. Zhang, and Y.-C. Zheng, in *Proceedings of the 27th ACM International Conference on Architectural Support for Programming Languages and Operating Systems* (2022), 10.1145/3503222.3507761.

[7] J. M. Gambetta, A. D. Córcoles, S. T. Merkel, B. R. Johnson, J. A. Smolin, J. M. Chow, C. A. Ryan, C. Rigetti, S. Poletto, T. A. Ohki, M. B. Ketchen, and M. Steffen, Phys. Rev. Lett. **109,** 240504 (2012).

[8] D. C. McKay, S. Sheldon, J. A. Smolin, J. M. Chow, and J. M. Gambetta, Phys. Rev. Lett. **122,** 200502 (2019).

[9] M. Sarovar, T. Proctor, K. Rudinger, K. Young, E. Nielsen, and R. Blume-Kohout, Quantum **4,** 321 (2020).

[10] K. Rudinger, C. W. Hogle, R. K. Naik, A. Hashim, D. Lobser, D. I. Santiago, M. D. Grace, E. Nielsen, T. Proctor, S. Seritan, S. M. Clark, R. Blume-Kohout, I. Siddiqi, and K. C. Young, PRX Quantum **2,** 040338 (2021).

[11] Z. Chen, K. J. Satzinger, J. Atalaya, A. N. Korotkov, A. Dunsworth, D. Sank, C. Quintana, M. McEwen, R. Barends, P. V. Klimov *et al.*, Nature (London) **595,** 383 (2021).

[12] P. Parrado-Rodrí guez, C. Ryan-Anderson, A. Bermudez, and M. Müller, Quantum **5,** 487 (2021).

[13] C. Ospelkaus, C. E. Langer, J. M. Amini, K. R. Brown, D. Leibfried, and D. J. Wineland, Phys. Rev. Lett. **101,** 090502 (2008).

[14] E. Urban, T. A. Johnson, T. Henage, L. Isenhower, D. Yavuz, T. Walker, and M. Saffman, Nat. Phys. **5,** 110 (2009).

[15] J. M. Auger, S. Bergamini, and D. E. Browne, Phys. Rev. A **96,** 052320 (2017).

[16] H. Levine, A. Keesling, A. Omran, H. Bernien, S. Schwartz, A. S. Zibrov, M. Endres, M. Greiner, and V. Vuletić, and M. D. Lukin, Phys. Rev. Lett. **121,** 123603 (2018).

[17] C. Fang, Y. Wang, S. Huang, K. R. Brown, and J. Kim, Phys. Rev. Lett. **129,** 240504 (2022).

[18] P. Krantz, M. Kjaergaard, F. Yan, T. P. Orlando, S. Gustavsson, and W. D. Oliver, Appl. Phys. Rev. **6,** 021318 (2019).

[19] A. Ash-Saki, M. Alam, and S. Ghosh, IEEE Trans. Quantum Eng. **1,** 1 (2020).

[20] A. Kandala, K. X. Wei, S. Srinivasan, E. Magesan, S. Carnevale, G. A. Keefe, D. Klaus, O. Dial, and D. C. McKay, Phys. Rev. Lett. **127,** 130501 (2021).

[21] P. Zhao, K. Linghu, Z. Li, P. Xu, R. Wang, G. Xue, Y. Jin, and H. Yu, PRX Quantum **3,** 020301 (2022).

[22] D. Buterakos, R. E. Throckmorton, and S. D. Sarma, Phys. Rev. B **97,** 045431 (2018).

[23] I. Heinz and G. Burkard, Phys. Rev. B **105,** 085414 (2022).

[24] R. E. Throckmorton and S. Das Sarma, Phys. Rev. B **105,** 245413 (2022).

[25] P. Mundada, G. Zhang, T. Hazard, and A. Houck, Phys. Rev. Appl. **12,** 054023 (2019).

[26] J. Ku, X. Xu, M. Brink, D. C. McKay, J. B. Hertzberg, M. H. Ansari, and B. L. T. Plourde, Phys. Rev. Lett. **125,** 200504 (2020).

[27] P. Zhao, P. Xu, D. Lan, J. Chu, X. Tan, H. Yu, and Y. Yu, Phys. Rev. Lett. **125,** 200503 (2020).

[28] A. R. R. Carvalho, H. Ball, M. J. Biercuk, M. R. Hush, and F. Thomsen, Phys. Rev. Appl. **15,** 064054 (2021).

[29] K. X. Wei, E. Magesan, I. Lauer, S. Srinivasan, D. F. Bogorin, S. Carnevale, G. A. Keefe, Y. Kim, D. Klaus, W. Landers *et al.*, Phys. Rev. Lett. **129,** 060501 (2022).

[30] V. Tripathi, H. Chen, M. Khezri, K.-W. Yip, E. M. Levenson-Falk, and D. A. Lidar, Phys. Rev. Appl. **18,** 024068 (2022).

[31] C. Zhang, Y. Chen, Y. Jin, W. Ahn, Y. Zhang, and E. Z. Zhang, arXiv:2009.02346.

[32] B. Zhang, S. Majumder, P. H. Leung, S. Crain, Y. Wang, C. Fang, D. M. Debroy, J. Kim, and K. R. Brown, Phys. Rev. Appl. **17,** 034074 (2022).

[33] D. Dong and I. R. Petersen, IET Control Theory Appl. **4,** 2651 (2010).

[34] T. J. Green, J. Sastrawan, H. Uys, and M. J. Biercuk, New J. Phys. **15,** 095004 (2013).

[35] H. Ball and M. J. Biercuk, Eur. Phys. J. Quantum Technol. **2,** 11 (2015).

[36] F. K. Wilhelm, S. Kirchhoff, S. Machnes, N. Wittler, and D. Sugny, arXiv:2003.10132.

[37] D. d'Alessandro, *Introduction to Quantum Control and Dynamics* (Chapman and Hall/CRC, London, 2021), 10.1201/9781003051268.

[38] Y. Oda, D. Lucarelli, K. Schultz, B. D. Clader, and G. Quiroz, Phys. Rev. Applied **19,** 014062 (2023).

[39] L. Viola, E. Knill, and S. Lloyd, Phys. Rev. Lett. **82,** 2417 (1999).

[40] M. Biercuk, A. Doherty, and H. Uys, J. Phys. B **44,** 154002 (2011).

[41] Daniel A. Lidar and Todd A. Brun, *Quantum Error Correction* (Cambridge University Press, Cambridge, England, 2013).

[42] B. Pokharel, N. Anand, B. Fortman, and D. A. Lidar, Phys. Rev. Lett. **121,** 220502 (2018).

[43] G. A. Álvarez and D. Suter, Phys. Rev. Lett. **107,** 230501 (2011).

[44] J. Bylander, S. Gustavsson, F. Yan, F. Yoshihara, K. Harrabi, G. Fitch, D. G. Cory, Y. Nakamura, J.-S. Tsai, and W. D. Oliver, Nat. Phys. **7,** 565 (2011).

[45] L. Cywiński, Phys. Rev. A **90,** 042307 (2014).

[46] L. M. Norris, G. A. Paz-Silva, and L. Viola, Phys. Rev. Lett. **116,** 150503 (2016).

[47] G. A. Paz-Silva, L. M. Norris, and L. Viola, Phys. Rev. A **95,** 022121 (2017).

[48] V. Frey, S. Mavadia, L. Norris, W. De Ferranti, D. Lucarelli, L. Viola, and M. Biercuk, Nat. Commun. **8,** 2189 (2017).

[49] Y. Sung, F. Beaudoin, L. M. Norris, F. Yan, D. K. Kim, J. Y. Qiu, U. von Lüpke, J. L. Yoder, T. P. Orlando, S. Gustavsson *et al.*, Nat. Commun. **10,** 3715 (2019).

[50] V. Frey, L. M. Norris, L. Viola, and M. J. Biercuk, Phys. Rev. Appl. **14,** 024021 (2020).

[51] U. von Lüpke, F. Beaudoin, L. M. Norris, Y. Sung, R. Winik, J. Y. Qiu, M. Kjaergaard, D. Kim, J. Yoder, S. Gustavsson, L. Viola, and W. D. Oliver, PRX Quantum **1,** 010305 (2020).

[52] L. Cywiński, R. M. Lutchyn, C. P. Nave, and S. Das Sarma, Phys. Rev. B **77,** 174509 (2008).

[53] L. M. Norris, D. Lucarelli, V. M. Frey, S. Mavadia, M. J. Biercuk, and L. Viola, Phys. Rev. A **98,** 032315 (2018).

[54] T. Chalermpusitarak, B. Tonekaboni, Y. Wang, L. M. Norris, L. Viola, and G. A. Paz-Silva, PRX Quantum **2,** 030315 (2021).

[55] See Supplemental Material at http://link.aps.org/supplemental/10.1103/PhysRevLett.131.210802, which includes Refs. [57–61], for further details on CSC extensions and CR protocols and demonstrations.

[56] Matt McEwen *et al.*, Nat. Phys. **18,** 107 (2022).

[57] Robin Harper, Steven T Flammia, and Joel J Wallman, Nat. Phys. **16,** 1184 (2020).

[58] Marcus Stollsteimer and Günter Mahler, Phys. Rev. A **64,** 052301 (2001).

[59] Gregory Quiroz and Daniel A Lidar, Phys. Rev. A **88,** 052306 (2013).

[60] Daniel A. Lidar, Adv. Chem. Phys. **154,** 295 (2014).

[61] E. J. Connors, J. Nelson, L. F. Edge, and J. M. Nichol, Nat. Commun. **13,** 940 (2022).

[62] W. Lawrie, M. Russ, F. van Riggelen, N. Hendrickx, S. de Snoo, A. Sammak, G. Scappucci, and M. Veldhorst, Nat. Commun. **14,** 3617 (2023).

[63] J. He, Q. Liu, Z. Yang, Q. Niu, X. Ban, and J. Wang, Phys. Rev. A **104,** 063120 (2021).

[64] G. Quiroz, P. Titum, P. Lotshaw, P. Lougovski, K. Schultz, E. Dumitrescu, and I. Hen, arXiv:2109.04482.

[65] J. Morris, F. A. Pollock, and K. Modi, Open Syst. Inf. Dyn. **29,** 2250007 (2022).

[66] Y.-Q. Chen, K.-L. Ma, Y.-C. Zheng, J. Allcock, S. Zhang, and C.-Y. Hsieh, Phys. Rev. Appl. **13,** 034045 (2020).

[67] G. A. White, C. D. Hill, F. A. Pollock, L. C. Hollenberg, and K. Modi, Nat. Commun. **11,** 6301 (2020).

[68] H. Zhang, B. Pokharel, E. M. Levenson-Falk, and D. Lidar, Phys. Rev. Appl. **17,** 054018 (2022).

[69] A. M. Souza, G. A. Álvarez, and D. Suter, Phys. Rev. A **85,** 032306 (2012).

[70] P. Wocjan, Phys. Rev. A **73,** 062317 (2006).

[71] R. Stine, Sociol. Methods Res. **18,** 243 (1989).

[72] N. Ezzell, B. Pokharel, L. Tewala, G. Quiroz, and D. A. Lidar, arXiv:2207.03670.

[73] K. Schultz, G. Quiroz, P. Titum, and B. D. Clader, Phys. Rev. Res. **3,** 033229 (2021).

[74] A. Murphy, J. Epstein, G. Quiroz, K. Schultz, L. Tewala, K. McElroy, C. Trout, B. Tien-Street, J. A. Hoffmann, B. D. Clader, J. Long, D. P. Pappas, and T. M. Sweeney, Phys. Rev. Res. **4,** 013081 (2022).